Anti-resonant based nested terahertz fiber design for illicit drugs detection

Shaymaa Riyadh Tahhan[1], Hadeel K. Aljobouri[2], **Baraa Riyadh Altahan**[3]
[1]Laser and Optoelectronics Engineering Department, College of Engineering, Al-Nahrain University, Baghdad, Iraq
[2]Biomedical Engineering Department, College of Engineering, Al-Nahrain University, Baghdad, Iraq
[3]Medical Instrumentation Techniques Engineering Department, Al-Mustaqbal University College, Babil, Iraq

Article Info

ABSTRACT

Anti-resonant hollow-core fibers (AR-HCFs) have gotten a lot of interest lately because of their potential uses in different medical sensing applications. In this work, an anti-resonant THz fiber (ATF) biosensor is implemented to check for illicit drugs and identify them at airport borders. Three different unlawful medicines have been chosen for the proposed design, Cocaine, Amphetamine, and Ketamine. A novel hollow-core anti-resonant fibers (HC-ARF) Matryoshka shape sensor has been designed for detecting the illegal drugs. The proposed design shows a robust sensitivity ranging from 99.8-99.9% and shallow confinement losses compared to other articles in the same field, as the higher losses are 9.3×10^{-4} dB/m with cocaine. Bending loss lessens as the bending radius rises while it is still below 1 dB/cm for radius more than 10 cm. The numerical simulation outcomes displayed that the designed HC-ARF has 0.0643 ± 0.0238 ps/THz/cm flat dispersion at 0.6-2 THz. As the first application in this field, this work will be the first published in the literature.

Corresponding Author:

Hadeel K. Aljobouri
Biomedical Engineering Department, College of Engineering, Al-Nahrain University
Baghdad 10072, Iraq
hadeel_bme77@yahoo.com

1. INTRODUCTION

Blood analysis is an appropriate window for detecting a person under the effect of illicit drugs. This method is usually measurable in minutes to hours versus one day to some days from saliva or urine [1]. Despite that, some places require rapid detection for these cases as in the airport or some sensitive places where more security is required. Remarkable work has been proposed and simulated using photonic crystal fiber (PCF) [2]–[4] in terahertz (THz) regime as a novel, accurate, and reliable technique for sensing illegal drugs in the blood [5]. Analogous to the previous work in [5], anti-resonant THz fiber (ATF) is proposed as a new design and application for sensing illegal drugs in the blood.

Fiber sensors have different applications in the field of biomedicine [6]–[10], but there is no application in the proposed field-based anti-resonant fiber design. Since the first appearance of the anti-resonant fiber in 2002, and due to its considerably reduced light-material connection, it has attracted a powerful technique due to its broad transmission bands [11]. Additionally, this technology has rampantly evolved in low-loss broadband transmission [4].

In 2015, Belardi [12] proposed to modify the design of the hollow-core anti-resonant fibers (HC-ARFs). He demonstrated that this technique provides fresh potential in the near-infrared. It also gives fast-responding for gas detection. The present technology offers more flexibility in constructing the HC-ARFs with short optical attenuation of the visible spectral regime and prolonged transmission bandwidth

in the near-infrared [12]. In Yan *et al.* [13] provided a new design based on high-birefringence hollow-core anti-resonant optical fiber and theoretically determined production parameters. They constructed the anti-resonant fiber simply by using ten Topas tubes only. Two big tubes were used to increase birefringence. High birefringence was achieved by raising the thickness and outer diameter of large tubes while reducing the thickness of tiny tubes, according to the production effects.

In contrast to this benefit, the introduced construction could cause a decrease in bandwidth and an increase in loss [13]. Based on the anti-resonant waveguiding process, Xiao *et al.* [14] suggested a low-loss polarization-maintaining hollow-core fiber in 2019. The presented THz fiber design was with four half-elliptical cladding membranes. They detected significant effects on modal properties by modifying the core dimension, size, and shape of cladding membranes [14]. Truong *et al.* [15] published a mathematical and experimental validation of a wireless power transfer system (WPTS) with magnetic coupling in 2019. WPTS operated at the resonance and antiresonance frequencies of both the receiver and transmitter. A theoretical model based on circuit theory was advanced. The whole model was proved experimentally and then used for numerical examinations [15]. In Mollah *et al.* [16] proposed a zeonex-based loss HC-ARF for polarization filtering (PF) application in the THz spectral range. They used the finite element technique with the designed THz fiber. This method is a practical and precise computational for calculating the modal properties of the fiber [16]. In Mitu *et al.* [17] proposed using a negative curving hollow-core (NC-HC) fiber as a magnetic field sensor. The NC-HC fiber involved five nested rings. Pure silica was used in the presented fiber design, and it was filled with magnetic fluid. The magnetic fluid's refractive index (RI) differs from the neighboring magnetic field strength changes. The managing properties of the sensor were tested by COMSOL multiphysics software. The presented sensor had proper properties, such as low loss, liquid infiltration feasibility, and high sensitivity. Thus, it was successfully used in standard factors, like strain, displacement, temperature, liquid level and magnetic sensor [17].

Due to the presented unique characteristics, the anti-resonant biosensor is proposed and implemented as a new application for sensing drugs or alcohol in individuals. Illegal drugs are divided into some groups, and the stimulants group has been proposed in this work for sensing by the designed ATF. Cocaine (n=1.5022) [18], Amphetamine (n=1.518) [19], and Ketamine (n=1.562) [20] are selected as illegal drugs within the stimulus group, which has refractive indices around 1.5 [21]. These drugs have different acute effects and health risks on the individuals, such as high blood pressure, heart rate, body temperature, energy, tremors, reduced appetite, weight loss, cardiac or cardiovascular complications, seizures, stroke, addiction [22].

The suggested fiber can be made using existing fabrication equipment since it has realistic manufacturing parameters. As a result, the suggested sensor might be employed as a chemical sensor, particularly in the medical, food, and industrial sectors, as the three compounds stated above have significant medicinal implications. The present manufacturing technology allows for the realistic implementation of this proposed hollow-core node-less negative-curvature fiber (HC-NNCF) sensor. As a result, the suggested terahertz sensor might be a good choice for opto-fluidic sensing applications in culinary, healthcare, and industrial chemical research. Capillary stack and draw, 3D printing, and extrusion are the most prevalent methods for fabricating negative curvature hollow core fibers (NC-HCFs). The stack and draw approach may be used to make simple NC-HCF, nested NC-HCF, and even conjoined-tube NC-HCF. 3D printing also allows for the fabrication of more complicated structures with a larger cladding thickness. On the other hand, fabricates a THz NC-HCF with a cladding tube thickness of 0.092 mm. As a result, the suggested fiber should likewise be manufactured utilizing existing fabrication procedures [23], [24].

Stack and draw, drilling, capillary stacking and extrusion, 3D printing, and other commercially accessible fiber production processes have all been employed for a long time. Recent advances in 3D printing technology have made it easier to create complicated asymmetrical structures. Several researchers used the stack and draw approach to manufacture a micrometer-based basic HC-NNCF. The stack and draw approach has recently been used to build complicated nested and co-joined HC-NNCF structures. This suggested HC-NNCF sensor may thus be made utilizing the existing stack and draw methods [25], [26].

In this article, an anti-resonant biosensor is implemented to check for unlawful drugs and identify them at airport borders. As the first application in this field, this work will be the first published in the literature. The rest of this essay will be organized as: the geometrical model of the proposed design is shown in section 2. The physical characterization of the proposed design and the numerical analysis are presented in sections 3 and 4, respectively. The outcomes and commentary are presented in sections 5 and 6, respectively. The paper comes to a close with section 7.

2. MODEL DESIGN

The presented structure design of the proposed model is based on the selection of different capillary tubes. Three attempts of structural design are presented in this work. In the first attempt, the structural design

used six circular tubes. Through this design, the light propagation through the tubes suffers from scattering. So, the circular tubes are changed with a circle design. The circle tubes provided enhanced results than the previous design. The differences between the circular and circle nested structures are considered a final step to an optimal arrangement between the proposed methods. The presented structure is designated by examining their sensitivity and loss values responses based on illegal drugs absorption spectroscopy for 1.0 to 2.0 THz mainly to detect cocaine, Ketamine, and amphetamine drugs. As a result, the nested circular capillaries have superior responses to the other arrangements.

The parameters (D_c, r_1, r_2, t, and t_1) are selected by tuning their values, as shown in Figure 1(a). Where (D_c) is the core diameter, ($d=2r_1$) is the interior tube gaps, The two circles with radius (r_1 and r_2) and a wall thickness (t_1) were united to form like a matryoshka doll geometry which represents nested cladding tube (shape a). The primary cladding tube (shape b) is formed from resizing (shape a) isotopically by 0.68. The sensing material is injected in the core region and interior tube gaps for sensitivity testing as indicated with the gray area in Figure 1(b). While both matryoshka tubes are filled with air, and the wall thickness is filled with Topas.

(a)   (b)
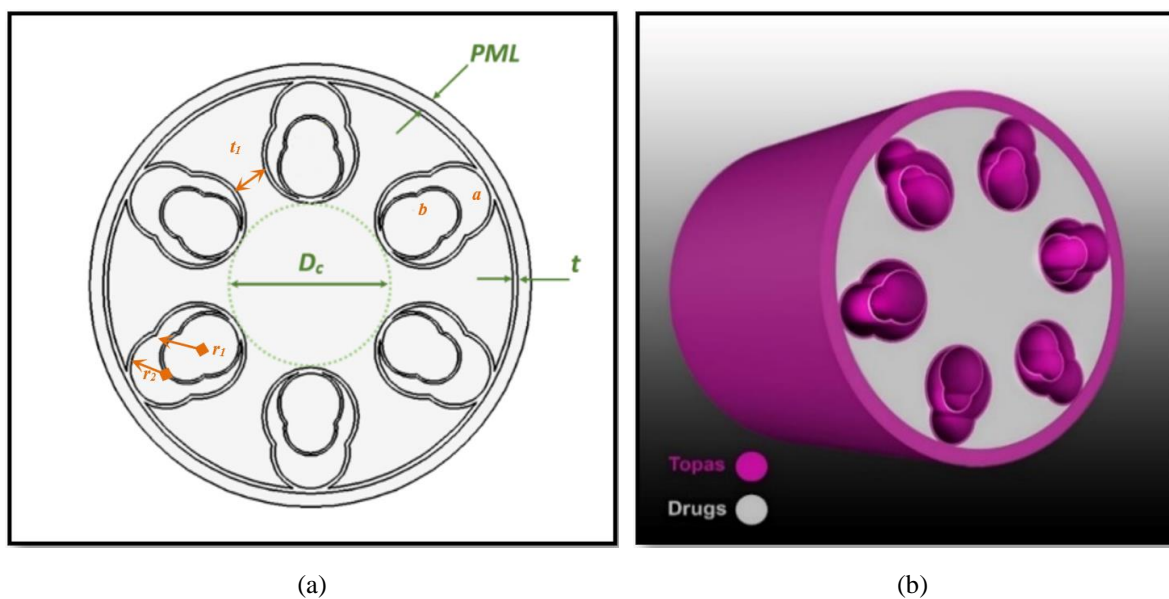
Figure 1. The proposed biosensor PCF (a) cross-sectional geometry of the Matryoshka structure ARN-PCF and (b) 3D ARN-PCF geometry representation with Topas and drugs filling area

3. PHYSICAL CHARACTERIZATION OF THE PROPOSED NESTED FIBER

In this work, a novel HC-ARF has a hollow core with six non-touching Matryoshka doubled by scale down as cladding. The finite element technique (FEM) constructed simulation software COMSOL multiphysics is used for solving the double curl Maxwell's equation. The first ten modes of the complex refractive indices have been solved to describe the proposed design. The relative repair tolerance is 1×10^{-6}, while the number of degrees of freedom is solved for 164,097. Finalized geometry has 15 domains, 232 boundaries, and 232 vertices as shown in Figure 2 13% width of the entire THz fiber diameter is hosted outer the margin of the cladding as a circular perfectly matched layer (PML). The PML design gives an advantage of absorbing backscattering at the simulation region's edges.

During the simulation, the bulk material absorption loss of Topas is measured as $\alpha_{mat}=0.20$ cm^{-1}. Dry air is used as the transparent environment for THz waves design. Air is the best-used transparent environment because it's negligible absorption ($\alpha_m \approx 0$) in THz frequency bands. So, this value has been disregarded in the calculation of other losses. The intensity distributions of basic (LP01) and higher-order (HOM: LP31) core modes are shown in Figure 2(a). The contour lines of the equivalent computed magnetic field distribution profiles at 1 THz for $d/D=0.995$ are highlighted in Figure 2(b). A minimal amount of power escapes towards cladding for LP01 due to the dominating fundamental core mode. The LP31 exhibits a strong power-cladding interaction to introduce higher-order suppression (HOM).
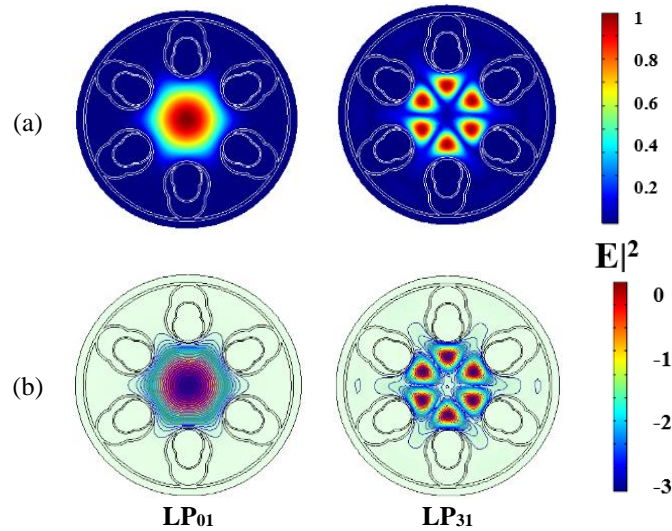
Figure 2. The electric and magnetic field mode (a) electric field mode (rainbow) and (b) magnetic field polarization (contour) for both LP01 and LP21 with Dc=3.76 mm and t=0.09 mm at 1 THz

4.   NUMERICAL ANALYSIS

For a precise simulation of material diffusion, Topas through a refractive index of 1.5258 valid in the frequency variety of 0.1 to 2 THz is utilized in this design [27]. For an accurate study of sensing properties of the presented sensor, a comprehensive perfectly matched layer (PML) edging technique is employed through the following equations for ending vector components, wavelength sensitivity, valued confinement loss, and amplitude sensitivity.

The relative sensitivity is calculated as (1) to test the sensing performance of the considered photonic crystal fiber (PCF) [28]:

$$r = \frac{n_r}{n_{eff}} \times \eta', \tag{1}$$

where n_{eff} denotes the guided mode's effective RI, n_r denotes the actual amount of the targeted analyte's RI for sensing [28], and η' represents the core power fraction. The amount of power that propagates in the core hollow discontinuities is designated by the core power fraction and considered as [29]:

$$\eta' = \frac{\int_x S_z \, dA}{\int_{all} S_z \, dA} \times 100 \, \% \tag{2}$$

where S_z is the Poynting vector's z component, the denominator is estimated for all spaces of the fiber, and over the core area, the numerator is integrated, as in effective material loss (EML) numeration.

Since the loss properties of the PCF are is a significant major, EML and confinement loss are the two primary loss processes. EML develops when the bulk material absorbs incident THz light, and excessive EML standards can influence the fiber's propagation length. The (3) describes the EML (α_{eff}) of the proposed hybrid fiber [30]:

$$\alpha_{eff} = \sqrt{\frac{\varepsilon_0}{\mu_0}} \left(\frac{\int_{mat} n_{mat} |E|^2 \alpha_{mat} dA}{2 \int_{All} S_z dA} \right), cm^{-1} \tag{3}$$

where μ_0 represents vacuum permeability, ε_0 represents vacuum permittivity, α_{mat} represents bulk material absorption loss, n_{mat} represents the material refractive index, and S_z is the z component of the Poynting vector. $S_z = 1/2 \, Re|E \times H|$, where H and E are the magnetic field component's complex conjugate and electric field, respectively. The numerator integral is calculated over the bulk material area, while the denominator integral is calculated over the entire cross-section of the fiber. The degree of light localization at the core is designated by confinement loss (Lc), contingent on the core region's optical density. Light scatters across the cladding when confinement loss is rising, overcoming the estimated response. Confinement loss is calculated as [31]:

$$L_c = 8.686 \times \frac{2\pi}{\lambda} \times \text{Im}(n_{\text{eff}}), \quad (\text{dB/cm}), \tag{4}$$

where *Im (neff)* is the imaginary component of the fundamental mode's effective refractive index, and λ is the practical wavelength.

Dispersion is a key element that influences THz wave transmission via pulse broadening. As a result, a minimal and flat dispersion profile is all the time recommended, making the fiber suited for far reaching communication. Because the because Topas' RI is constant, material dispersion's contribution to chromatic dispersion can be ignored. As a result, the suggested fiber's total dispersion will be simply the set velocity dispersion (β_2) and may be written as [30], [32]

$$\beta_2 = \frac{dn_{eff}}{d\omega}\frac{2}{c} + \frac{\omega}{c}\frac{d^2 n_{eff}}{d^2\omega}, \quad (\text{ps/THz/cm}), \tag{5}$$

where c and n_{eff} are the light speed and effective refractive index, respectively, and angular frequency is ω. Another essential characteristic to consider is a fiber's bending loss. When a linear fiber is replaced with a bent fiber using the conformal transformation technique, an equitable refractive index is employed [32]:

$$n^{`} = n(x,y)\left(1 + \frac{S}{R}\right), \tag{6}$$

where S is the bending direction (x or y), and R is the bending radius, where $n(x, y)$ and n' are the linear fiber RI before and after bending, respectively.

5. RESULTS

Figures 3(a) and 3(b) demonstrate the impact of modifying core diameter (D_c) and inner clad capillary (d) diameter on loss and effective refractive index for both core fundamental mode LP01 and HOM LP31. A larger core (D_c) and clad capillary (d) diameter lead to reduced losses, as seen in Figure 3(a). The effective index for LP01 is straight compared to the HOM one, which increased with increasing the core diameter and proportional to the inner clad capillary diameter increasing.

At the same time, more significant D_c and d can result in increased sensitivity, as demonstrated in Figure 3(b). However, fiber compactness is influenced by the entire diameter of the fiber. The fiber should be as thin as feasible in order to be both adaptable and small. Consequently, the core and cladding capillary radii have been adjusted to 2.00 mm and 0.82 mm, respectively.
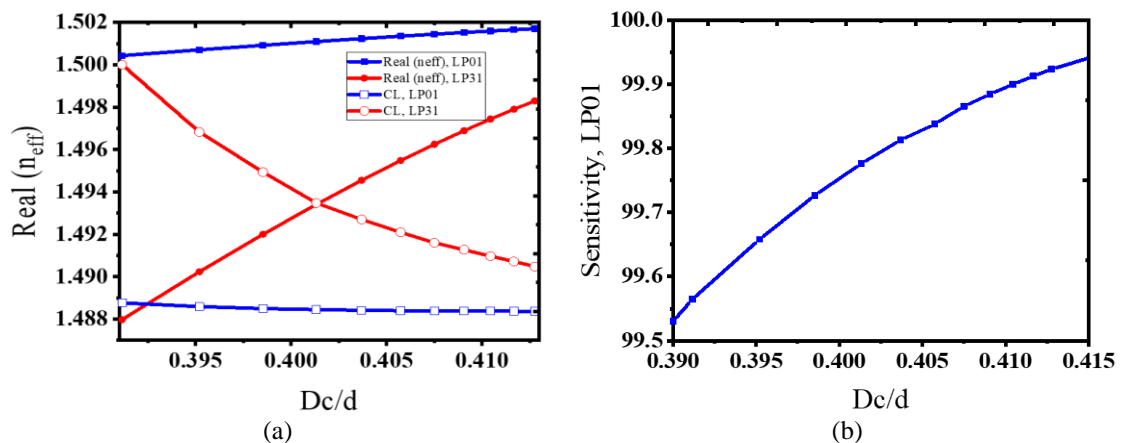
Figures 3. The impact of modifying Dc and inner clad capillary d on loss and effective refractive index for both core fundamental mode LP01 and HOM LP31 (a) reduced losses due to larger D_c and clad capillary d and (b) increased sensitivity due to D_c and d

The ratio of the amount of light propagates in the drugs of the diffracted limited mode LP01 within the core region to the total light power, addressed as a core power fraction. Figures 4(a) and 4(b) depict the temporal core power fraction distribution and the relative sensitivity of the suggested AR-PCF for the before

stated examines (cocaine, amphetamine, and Ketamine). The core power fraction incrementally increases with the frequency expansion for any evaluates. Due to the improved core-cladding refractive index, a high drug refractive index indicates a substantial quantity of fractional power curving in the core analyses holes. The deflection in the fractional power movement over the core section of the PCF for the cocaine material is due to its lower refractive index value compared to the other two drugs. The relative sensitivity is proportional consistently to the fractional power due to their relationship. The most significant relative sensitivity values are 99.9711%, 99.9703%, and 99.98% for Cocaine, Amphetamine, and Ketamine, respectively.
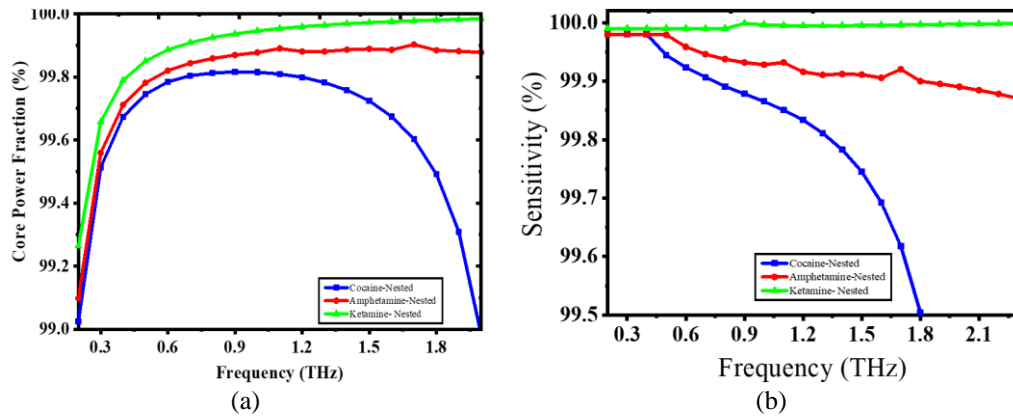
Figure 4. The temporal core power fraction and relative sensitivity (a) core power fraction (b) percentage sensitivity with frequency for three drugs

Material absorption loss is the most common form of loss in THz fiber (also known as an effective material loss). In particular, as illustrated in Figure 5, y-polarization results in quite a minimal EML loss. At 0.6 THz, cocaine drugs had the lowest EML of 0.03 dB/m. For both amphetamine and ketamine drugs, the suggested nested fiber has a lower EML. On 1.4 THz, the EML for Amphetamine is 0.0214 dB/cm, while at 2.1 THz, it is 0.0027 dB/cm. Due to the high incidence of electromagnetic radiation and the reliance of Topas material on THz frequency, EML decreases with frequency. At the same time, when compared to the other two substances, cocaine has a shallow refractive index. EML is rising at 1.2 THz for cocaine because light scatters into the cladding, implying that both core power and sensitivity will be reduced. For both amphetamine and Ketamine, the material loss is constant.
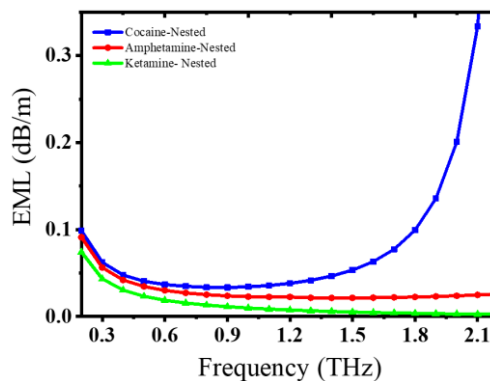
Figure 5. EML versus frequency for cocaine, amphetamine, and ketamine

Figure 6 depicts the losses of y-polarization modes as a function of frequency for each of the three drugs. In the frequency domain of 0.2 to 2.4 THz, there are two transmission windows for cocaine (blue line), as indicated. The first transmission window has a frequency domain of 0.2 to 1.4 THz, whereas the second transmission window has a frequency domain of 1.5 to 2.4 THz. The resonance frequencies for sensing

cocaine are 0.7 and 1.9 THz. When the frequency rises to the resonance frequency, the y-polarization losses increase and then diminish, and this process repeats in the following transmission window. Where the losses are 0.03 dB/cm at 0.7 THz and 0.01 dB/cm at 1.9 THz. For Amphetamine (red line), the peak losses of y-polarization mode are 0.0187 dB/cm at 1.2 THz resonance frequency. Because all the light is contained to the center, ketamine has no resonance frequency. As the wavelength gets shorter, it diminishes exponentially. PCF aids to improved performance when the confinement losses are minimal.

When confinement loss (CL) and effective material loss (EML) are added together, the overall loss is computed. The CL controls the total loss in anti-resonance fiber, despite solid or porous core fiber [16]. As demonstrated in Figure 7, the proposed HC-ARF achieves a low total loss of 0.0325 dB/m at 1.1 THz for cocaine drugs. It also reaches 0.0221 and 0.00152 dB/m at 1.6 and 2.7 THz, respectively, for Amphetamine and Ketamine medicines. Furthermore, with a frequency domain of 1.3 to 1.1 THz, vertical polarization mode (VPM) for Amphetamine has a frequency bandwidth of 200 GHz and losses of less than 2 dB/m.
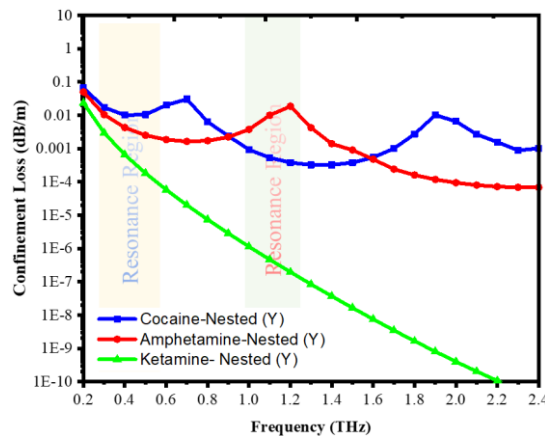
Figure 6. Confinement loss against frequency for cocaine, amphetamine, and ketamine
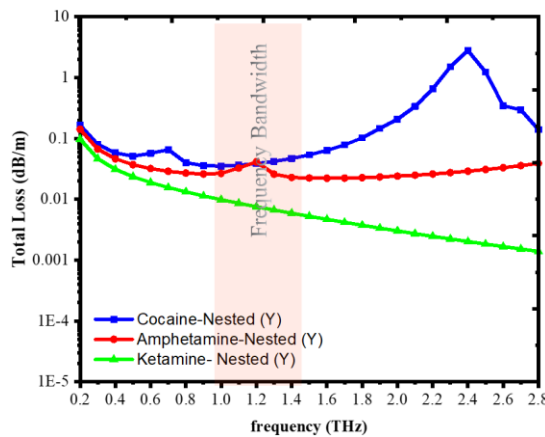
Figure 7. The total loss for the suggested HC-ARF as a function of the frequency, for all the investigated drugs

Figures 8(a) to 8(d) shows a theoretical comparison between three injectable drugs with different refractive indices. Because of the identical core diameter, the core mode effective index has virtually the same behavior throughout every medicine. Ketamine's effective refractive indices are substantially higher than amphetamine and cocaine. Consequently, the suggested structure's coupling between core modes and ketamine is stronger. This explains why, as shown in Figure 9 decreasing the cladding capillary hole can minimize bending loss. The sign of dispersion changes from positive to negative when the frequency of anti-resonant fibers climb within the transmission range. The dispersion curve shows a zero point at f=1.7 THz, which is on the transmission window's shorter wavelength side.
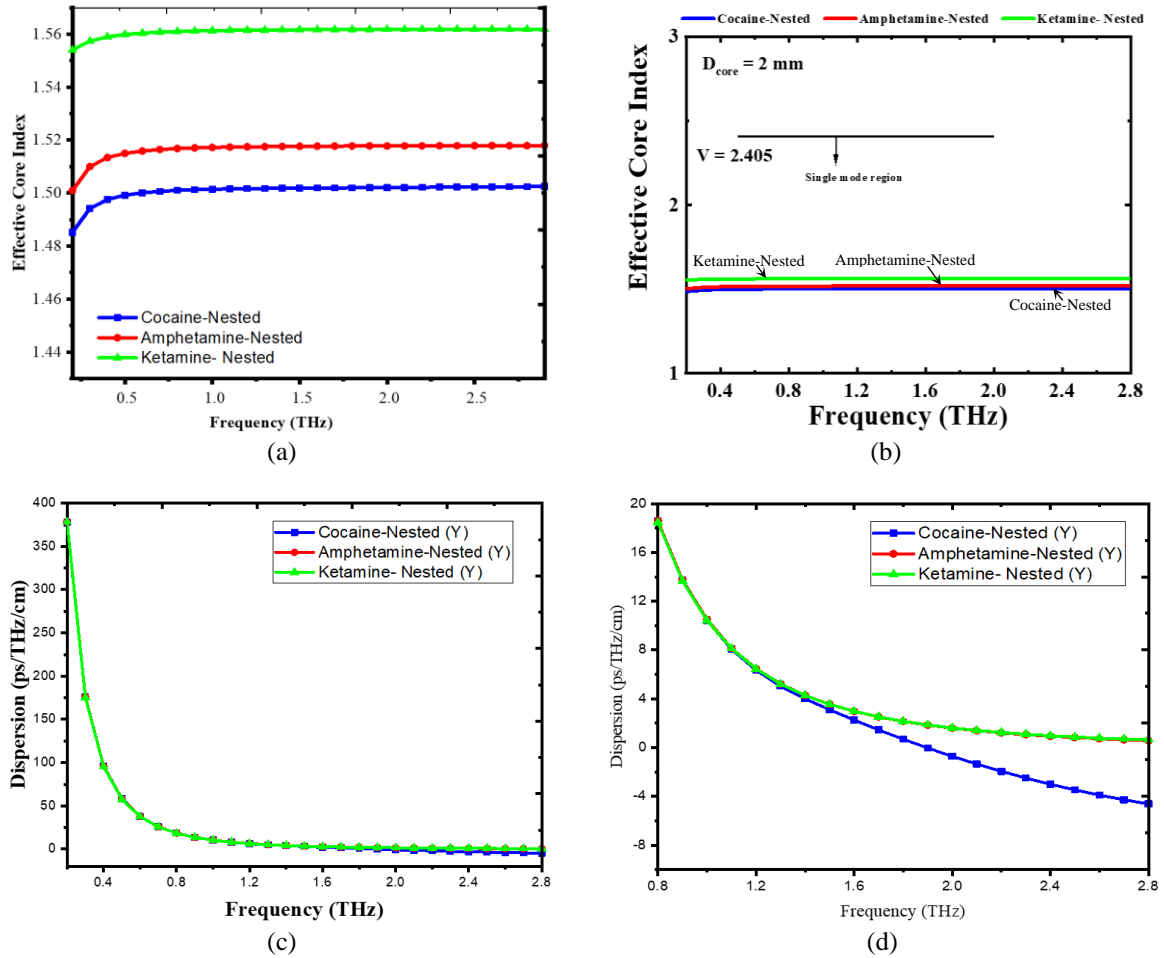
Figure 8. Comparison between three injectable drugs with different refractive indices (a) and (b) the effective RI of the suggested HC-ARF as a function of frequency for core diameter (Dc) of 2.00 mm, inner capillary d of 0.82 mm and thickness (t) of 0.09 mm, (c) and (d) the dispersion for the considered fiber as a function of THz frequency
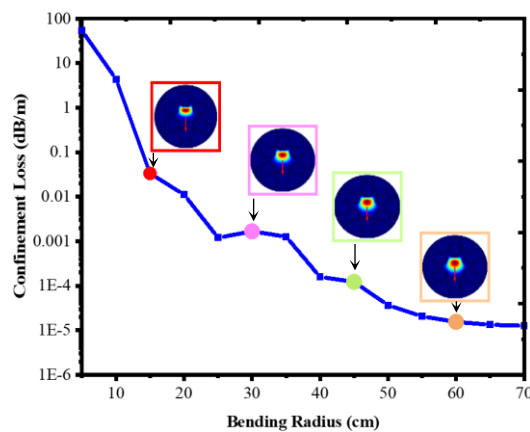
Figure 9. The designed fiber's bending radius as a function of THz frequency

The group velocity dispersion profile as a function of frequency for the three different medicine fillings is analyzed, as shown in Figure 9. The near zero-dispersion wavelength (ZDW) changes to higher frequencies as the refractive index rises. However, because of the slight anomalous dispersion throughout the spectrum, the ZDW moves further than ANFs when not filled. According to the behavior shown, the

suggested fiber has a minimal and flat dispersion of 0.0643±0.0238 ps/THz/cm at 0.6-2 THz. At 0.6-2 THz, the recommended fiber exhibits a minimum and flat dispersion of 0.0643 0.0238 ps/THz/cm.

The bending loss for bending radiuses ranging from 5 to 70 cm is depicted in Figure 9 in the *y-bend plane*. The plane's orientation is highly significant concerning the organization of the air holes structures [33]. The bending losses are 0.011 at 20 cm and 0.0012 for 25 cm for *Y* polarized mode. As predicted, bending distance decreases with increasing bending radius, which is the ratio between cladding and core structure size. However, for *R* more than 10 cm, the bending loss is less than 1 dB/m.

6. DISCUSSION

Table 1 compares the proposed HC-ARF to previous HC-ARF designs in terms of performance. The fiber released in [13] has the uppermost birefringence and the most significant loss. On the other hand, the fiber described in [14] has a somewhat lower loss but a lower birefringence than the fiber reported in [13]. It should be noted that EML was not taken into account in [13], [14], [34], even though it has an important influence on THz wave propagation.

Table 1. Performance comparison of the proposed HC-ARF with other HC-ARFs

Ref.	Background Material	Wavelength or frequency	Analyte	Confinement Losses	Sensitivity	EML	Birefringence	Bending Losses	Dispersion
[5]	Topas	1 THz	cocaine, amphetamine, ketamine	3.1083×10^{1}, 2.583×10^{-13}, 2.5801×10^{-13}	79.840%, 80.256%, 81.417%	0.00336, 0.00333, 0.09835	-		
[13]	Topas	2.34 THz		1.68			$>7\times10^{-4}$		
[17]	Pure Silica	0.65μm, 0.75μm, 0.9μm	magnetic strength of 200 Oe.	6.98018×10^{-9} 3×10^{-6}	2-6.8 nm/Oe		-	3.16×10^{-12} R_b=25 cm for X Polarization. 3.45×10^{-12} R_b=20 cm for Y Polarization.	
[14]	Zeonex	0.9 THz		0.50		$>10^{-4}$			
[32]	Topas	0.8-1.2 THz		/	/	0.0557	0.0595	10^{-4} at R_b=1.2 mm	0.09±0.28
[35]	Zeonex	1.00 THz	water, ethanol, benzene	7.20×10^{-03}, - -	99.04% - -	0.00114, - -	-	-	-
[36]	Zeonex	0.8 to 1.3 THz 1.44 THz	chloroform, polylactic acid, CCL3, glycerin, and benzene	For air filled 10^{-04}, About 0.01	99.19%, 99.46%, 99.48%, 99.65%, and 99.86%	10^{-03}, About 0.01	-	-	-
This work	**Topas**	**1 THz**	**cocaine, amphetamine, ketamine**	**9.3×10^{-12} 0.00375 1.136×10^{-6}**	**99.86% 99.93% 99.99%**	**0.034 0.0229 0.0098**	**10^{-9}**	**0.011 R_b=20 cm for Y Polarization. 0.0012 R_b=25 cm for Y Polarization.**	**0.0643± 0.0238 at 0.6-2 THz.**

7. CONCLUSION

Antiresonance fiber optic is designed and implemented for illegal drugs sensing. Despite the blood, analysis is an appropriate window for detecting the effect of illicit drugs. Still, some places need rapid detection for these cases, such as in the airport or sensitive areas that need more safety. Increased sensitivity can be achieved by increasing both core and clad capillary diameters. Fiber compactness, on the other hand, is impacted by the fiber's total diameter. The capillary radii of the core and cladding have been modified to 2.00 and 0.82 mm, respectively. The suggested fiber has a significant high sensitivity, which is 99.86527, 99.92808, and 99.99633% for cocaine, amphetamine, and ketamine, respectively. The summation of CL and EML concludes the overall loss. For cocaine drugs, the suggested HC-ARF has a total loss of 0.0325 dB/m at 1.1 THz. Amphetamine and Ketamine drugs have 0.0221 and 0.00152 dB/m at 1.6 and 2.7 THz. At 0.6-2 THz, the recommended fiber exhibits a minimum and flat dispersion of 0.0643±0.0238 ps/THz/cm. The bending distance reduces as the bending radius increases; yet, for R more than 10 cm, the bending loss is less than 1 dB/m.

REFERENCES

[1] Labcorp, "Workplace drug testing," *Lab. Corporation of America*. https://www.labcorp.com/organizations/employers/workplace-drug-testing (accessed Jun. 02, 2019).

[2] S. Tahhan, A. Ghazai, I. Alwan, and M. Ali, "Investigation of the characteristics of high-resistivity silica based hybrid porous core photonic crystal fiber for terahertz wave guidance," *Digest Journal of Nanomaterials and Biostructures*, vol. 14, no. 3, pp. 831–841, 2019.

[3] F. S. Al-Thahaby and A. A. Al-Dergazly, "Tuneable fiber bragg grating for magnetic field sensor," *Al-Nahrain Journal for Engineering Sciences*, vol. 20, no. 5, pp. 1112–1123, 2017.

[4] R. Fyath and Z. M. A. Kamil, "Investigation of raman amplification in photonic crystal fibers," *Al-Nahrain Journal for Engineering Sciences*, vol. 11, no. 3, pp. 511–521, 2008.

[5] S. R. Tahhan and H. K. Aljobouri, "Sensing of illegal drugs by using photonic crystal fiber in terahertz regime," *Journal of Optical Communications*, Mar. 2020, doi: 10.1515/joc-2019-0291.

[6] O. Tohyama, M. Kohashi, M. Fukui, and H. Itoh, "A fiber-optic pressure microsensor for biomedical applications," in *Proceedings of International Solid State Sensors and Actuators Conference (Transducers '97)*, 1997, vol. 2, pp. 1489–1492, doi: 10.1109/SENSOR.1997.635747.

[7] R. Otupiri, E. K. Akowuah, S. Haxha, H. Ademgil, F. AbdelMalek, and A. Aggoun, "A novel birefrigent photonic crystal fiber surface plasmon resonance biosensor," *IEEE Photonics Journal*, vol. 6, no. 4, pp. 1–11, Aug. 2014, doi: 10.1109/JPHOT.2014.2335716.

[8] A. Rahman, A. K. Rahman, and B. Rao, "Early detection of skin cancer via terahertz spectral profiling and 3D imaging," *Biosensors and Bioelectronics*, vol. 82, pp. 64–70, Aug. 2016, doi: 10.1016/j.bios.2016.03.051.

[9] D. Tosi, S. Poeggel, I. Iordachita, and E. Schena, "Fiber optic sensors for biomedical applications," in *Opto-Mechanical Fiber Optic Sensors*, Elsevier, 2018, pp. 301–333.

[10] W. Ni *et al.*, "Recent advancement of anti-resonant hollow-core fibers for sensing applications," *Photonics*, vol. 8, no. 4, Apr. 2021, doi: 10.3390/photonics8040128.

[11] F. Benabid, J. C. Knight, G. Antonopoulos, and P. S. J. Russell, "Stimulated raman scattering in hydrogen-filled hollow-core photonic crystal fiber," *Science*, vol. 298, no. 5592, pp. 399–402, Oct. 2002, doi: 10.1126/science.1076408.

[12] W. Belardi, "Design and properties of hollow antiresonant fibers for the visible and near infrared spectral range," *Journal of Lightwave Technology*, vol. 33, no. 21, pp. 4497–4503, Nov. 2015, doi: 10.1109/JLT.2015.2477775.

[13] S. Yan, S. Lou, X. Wang, T. Zhao, and W. Zhang, "High-birefringence hollow-core anti-resonant THz fiber," *Optical and Quantum Electronics*, vol. 50, no. 3, Mar. 2018, doi: 10.1007/s11082-018-1402-7.

[14] H. Xiao, H. Li, B. Wu, Y. Dong, S. Xiao, and S. Jian, "Low-loss polarization-maintaining hollow-core anti-resonant terahertz fiber," *Journal of Optics*, vol. 21, no. 8, Aug. 2019, doi: 10.1088/2040-8986/ab2d68.

[15] B. D. Truong, C. Roundy, E. Andersen, and S. Roundy, "Analysis of resonance and anti-resonance frequencies in a wireless power transfer system: analytical model and experiments," *IEEE Transactions on Circuits and Systems II: Express Briefs*, vol. 66, no. 7, pp. 1222–1226, Jul. 2019, doi: 10.1109/TCSII.2018.2878662.

[16] M. A. Mollah, S. Rana, and H. Subbaraman, "Polarization filter realization using low-loss hollow-core anti-resonant fiber in THz regime," *Results in Physics*, vol. 17, Jun. 2020, doi: 10.1016/j.rinp.2020.103092.

[17] S. A. Mitu *et al.*, "Novel nested anti-resonant fiber based magnetic fluids sensor: Performance and bending effects inspection," *Journal of Magnetism and Magnetic Materials*, vol. 538, Nov. 2021, doi: 10.1016/j.jmmm.2021.168230.

[18] PubChem, "Cocaine," *PubChem National Center for Biotechnology Information U.S. National Library of Medicine*. https://pubchem.ncbi.nlm.nih.gov/compound/Cocaine#section=pH (accessed Sep. 23, 2021).

[19] PubChem, "Amphetamine," *PubChem National Center for Biotechnology Information U.S. National Library of Medicine*. https://pubchem.ncbi.nlm.nih.gov/compound/Amphetamine#section=pH (accessed Sep. 23, 2021).

[20] PubChem, "Ketamine," *PubChem National Center for Biotechnology Information U.S. National Library of Medicine*. https://pubchem.ncbi.nlm.nih.gov/compound/Ketamine (accessed Dec. 17, 2021).

[21] W. M. Haynes, *CRC handbook of chemistry and physics*, 95th Editi. Amazon, 2014.

[22] NIH, "Commonly abused drugs," *National Institute on Drug Abuse*. Accessed Sep. 23, 2021. [Online]. Available: https://nida.nih.gov/sites/default/files/commonly_abused_drugs.pdf

[23] J. Sultana *et al.*, "Exploring low loss and single mode in antiresonant tube lattice terahertz fibers," *IEEE Access*, vol. 8, pp. 113309–113317, 2020, doi: 10.1109/ACCESS.2020.3003035.

[24] G. K. M. Hasanuzzaman, S. Iezekiel, C. Markos, and M. S. Habib, "Hollow-core fiber with nested anti-resonant tubes for low-loss THz guidance," *Optics Communications*, vol. 426, pp. 477–482, Nov. 2018, doi: 10.1016/j.optcom.2018.05.071.

[25] M. A. Mollah, M. S. Habib, and M. S. Habib, "Novel hollow-core asymmetric conjoined-tube anti-resonant fiber for low-loss THz wave guidance," *OSA Continuum*, vol. 3, no. 5, May 2020, doi: 10.1364/OSAC.393189.

[26] I. M. Ankan, M. A. Mollah, A. K. Paul, and K. Chakrabarti, "Polarization-maintaining and polarization-filtering negative curvature hollow core fiber in THz Regime," in *2020 IEEE Region 10 Symposium (TENSYMP)*, 2020, pp. 612–615, doi: 10.1109/TENSYMP50017.2020.9231018.

[27] K. Nielsen, H. K. Rasmussen, A. J. Adam, P. C. Planken, O. Bang, and P. U. Jepsen, "Bendable, low-loss Topas fibers for the terahertz frequency range," *Optics Express*, vol. 17, no. 10, May 2009, doi: 10.1364/OE.17.008592.

[28] I. K. Yakasai, P. E. Abas, S. Ali, and F. Begum, "Modelling and simulation of a porous core photonic crystal fibre for terahertz wave propagation," *Optical and Quantum Electronics*, vol. 51, no. 4, Apr. 2019, doi: 10.1007/s11082-019-1832-x.

[29] I. K. Yakasai, A. Rahman, P. E. Abas, and F. Begum, "Theoretical assessment of a porous core photonic crystal fiber for terahertz wave propagation," *Journal of Optical Communications*, vol. 43, no. 2, pp. 199–209, Apr. 2022, doi: 10.1515/joc-2018-0206.

[30] J. Luo *et al.*, "Design and numerical analysis of a THz square porous-core photonic crystal fiber for low flattened dispersion, ultrahigh birefringence," *Applied Optics*, vol. 56, no. 24, Aug. 2017, doi: 10.1364/AO.56.006993.

[31] M. A. Habib, E. Reyes-Vera, J. Villegas-Aristizabal, and M. S. Anower, "Numerical modeling of a rectangular hollow-core waveguide for the detection of fuel adulteration in terahertz region," *Fibers*, vol. 8, no. 10, Oct. 2020, doi: 10.3390/fib8100063.

[32] B. Wang, C. Jia, J. Yang, Z. Di, J. Yao, and J. Zhang, "Highly birefringent, low flattened dispersion photonic crystal fiber in the terahertz region," *IEEE Photonics Journal*, vol. 13, no. 2, pp. 1–10, Apr. 2021, doi: 10.1109/JPHOT.2021.3057698.

[33] R. M. Carter *et al.*, "Measurement of resonant bend loss in anti-resonant hollow core optical fiber," *Optics Express*, vol. 25, no. 17, Aug. 2017, doi: 10.1364/OE.25.020612.

[34] M. S. Habib, O. Bang, and M. Bache, "Low-loss single-mode hollow-core fiber with anisotropic anti-resonant elements," *Optics Express*, vol. 24, no. 8, Apr. 2016, doi: 10.1364/OE.24.008429.

[35] S. Hossain, A. Mollah, K. Hosain, and I. M. Ankan, "THz spectroscopic sensing of liquid chemicals using hollow-core anti-resonant fiber," *OSA Continuum*, vol. 4, no. 2, Feb. 2021, doi: 10.1364/OSAC.416921.

[36] I. M. Ankan, M. A. Mollah, J. Sultana, and M. S. Islam, "Negative curvature hollow-core anti-resonant fiber for terahertz sensing," *Applied Optics*, vol. 59, no. 28, Oct. 2020, doi: 10.1364/AO.395914.

BIOGRAPHIES OF AUTHORS

Shaymaa Riyadh Tahhan was born in the Iraqi city of Babylon in 1982. In 2003 and 2008, she got her B.Sc. and M.Sc. degrees in Laser and Optoelectronics Engineering from Al-Nahrain University in Baghdad, Iraq. In 2014, she earned a Ph.D. in electronics and communication engineering/laser applications from the University of Baghdad (theoretical) and Pittsburgh University (experimental), both in Baghdad, Iraq. Her career history includes experiences in optical fiber, spectroscopy, and laser systems laboratories. Optical fiber systems, particularly the manufacturing of fiber Bragg gratings (FBG) and photonic crystal fiber (PCF), as well as their use in sensors and as dispersion compensation in communication systems, are among her specific interests. She has worked at the Laser and Optoelectronics Engineering Department since 2016. She can be contacted at Shaymaa.Riyadh@gmail.com.

Hadeel K. Aljobouri received the B.S. degree in Biomedical Engineering from the University of Baghdad, Baghdad, Iraq, in 2000 the M.Sc. in Medical Engineering from Al-Nahrain University, Baghdad, Iraq, in 2004, and the Ph.D. at the Electrical and Electronics Engineering Department, Graduate School of Natural Science/Ankara Yıldırım Beyazıt University in Turkey. She worked as an Assistant Professor at the Biomedical Engineering Department at Al-Nahrain University in Iraq. Her research interests are biomedical signal processing, medical imaging, data mining, clustering techniques, and machine learning. She has many publications in the field of biomedical engineering. She can be contacted at email: hadeel_bme77@yahoo.com.

Baraa Riyadh Altahan born in the Iraqi city of Babylon in 1994, holds a bachelor's degree from the University's AL-MUSTAQBAL College in the field of computer technology engineering in 2016, and she also holds a master's degree from Imam Al-Rida International University in the field of software in 2021. She is an assistant lecturer in Medical Instrumentation Techniques Engineering Department, Al-Mustaqbal University College. She is working on Optical Fiber Sensors utilizing Finite Element Method and eager to expand her knowledge in this field. She can be contacted at Baraa.riyadh@mustaqbal-College.edu.iq.